



UNIVERSITY OF LEEDS

This is a repository copy of *Observation of spin-wave Doppler shift in Co₉₀Fe₁₀/Ru micro-strips for evaluating spin polarization*.

White Rose Research Online URL for this paper:

<https://eprints.whiterose.ac.uk/104352/>

Version: Accepted Version

Article:

Sugimoto, S orcid.org/0000-0003-0212-2805, Rosamond, MC, Linfield, EH et al. (1 more author) (2016) Observation of spin-wave Doppler shift in Co₉₀Fe₁₀/Ru micro-strips for evaluating spin polarization. Applied Physics Letters, 109 (11). 112405. ISSN 0003-6951

<https://doi.org/10.1063/1.4962835>

Published by AIP Publishing. This article may be downloaded for personal use only. Any other use requires prior permission of the author and AIP Publishing. The following article appeared in Sugimoto, S, Rosamond, MC, Linfield, EH and Marrows, CH (2016) Observation of spin-wave Doppler shift in Co₉₀Fe₁₀/Ru micro-strips for evaluating spin polarization. Applied Physics Letters, 109 (11). 112405. ISSN 0003-6951, and may be found at <https://doi.org/10.1063/1.4962835>. Uploaded in accordance with the publisher's self-archiving policy.

Reuse

Items deposited in White Rose Research Online are protected by copyright, with all rights reserved unless indicated otherwise. They may be downloaded and/or printed for private study, or other acts as permitted by national copyright laws. The publisher or other rights holders may allow further reproduction and re-use of the full text version. This is indicated by the licence information on the White Rose Research Online record for the item.

Takedown

If you consider content in White Rose Research Online to be in breach of UK law, please notify us by emailing eprints@whiterose.ac.uk including the URL of the record and the reason for the withdrawal request.



eprints@whiterose.ac.uk
<https://eprints.whiterose.ac.uk/>

Observation of spin-wave Doppler shift in Co₉₀Fe₁₀/Ru micro-strips for evaluating spin polarization

Satoshi Sugimoto,^{1,*} Mark C. Rosamond,² Edmund H. Linfield,²
and Christopher H. Marrows^{1,†}

¹*School of Physics & Astronomy, University of Leeds, Leeds, LS2 9JT, UK*

²*School of Electronic & Electrical Engineering, University of Leeds, Leeds, LS2 9JT,
UK*

(Dated: 09 September 2016)

The current-induced spin-wave Doppler shift has been investigated for Co₉₀Fe₁₀ films, with and without under- and overlayers of Ru, aiming to obtain quantitative insights into the value of spin polarization of the in a diffusive electrical currents flowing in this material. This extends the use of spin-wave Doppler shift spectroscopy beyond the study of Permalloy to other soft magnetic materials suitable for use in spintronic applications such as racetrack memories. The Damon-Eshbach spin-wave mode was employed, and a control experiment of Permalloy yielded a value of spin polarization of $P = 0.44 \pm 0.03$ for that material. An extended method to properly evaluate spin-wave Doppler shifts is developed that takes account of the non-negligible Oersted fields that are generated by the current density asymmetry caused by conducting under- or overlayers. The values of spin polarization for various Co₉₀Fe₁₀-based structures are found to lie in the range 0.3-0.35, only slightly less than in Permalloy.

PACS numbers: 85.75.-d, 75.40.Gb, 75.75.-c, 75.78.-n

*Electronic address: s.sugimoto@leeds.ac.uk

†Electronic address: c.h.marrows@leeds.ac.uk

Magnetic random access memory (MRAM) [1] and racetrack memory [2] are promising candidates for low power, high performance memories. Both technologies have a major difficulty in reaching commercial application in terms of the efficiency of generating spin angular momentum via electrical current injection. The key parameter is the spin polarization P that is expressed as $P = (J_{\uparrow} - J_{\downarrow}) / (J_{\uparrow} + J_{\downarrow})$, where J_{\uparrow} and J_{\downarrow} are the charge current densities carried by spin-up and spin-down electrons, respectively. In spin-transfer torque MRAM devices, the critical current density required to write a memory cell is proportional to $1/P$ [3]. The current spin polarization is also a key parameter in racetrack-type devices where the domain wall velocity is proportional to P [2,4]. In the search for highly spin polarized structures, research interest has shifted in stages, starting from soft in-plane ferromagnetic materials [5,6,7,8], toward out-of-plane magnetization structures [9,10,11] and systems with Dzyaloshinskii-Moriya interactions (DMI) [12,13] leading to chiral DWs [14, 15]. Most recently, there has been interest in pairs of magnetic layers coupled antiferromagnetically through Ru spacers [16]. Very high domain wall velocities have been achieved in perpendicularly magnetized synthetic antiferromagnets [17], whilst a remarkable reduction in the critical current density for domain wall motion has been observed for in-plane magnetized coupled domain walls in a $\text{Co}_{90}\text{Fe}_{10} / \text{Ru} / \text{Co}_{90}\text{Fe}_{10}$ synthetic ferrimagnet (SyF) track [18].

Various techniques have been developed to quantitatively evaluate P [19,20,21,22,23,24,25,26], nevertheless the same material can present different current spin polarizations in different transport regimes [27]. Racetrack memories operate in the diffusive regime, where the results of ballistic or tunneling experiments are not relevant. Methods developed in this regime include measurements of the current-perpendicular-to-plane giant magnetoresistance [28], domain wall resistance [29, 30], and depinning of domain walls through spin-transfer torque [31]. Here we adopt the current-induced spin-wave Doppler shift (CISDS) technique [32,33], which has the advantages of immunity to extrinsic effects such as interfacial effects at contacts.

The Landau-Lifshitz-Gilbert equation, in a form including adiabatic and non-adiabatic spin transfer torques, describes the interaction between spin waves and currents [34,35]. From it, the magnetization drift velocity \mathbf{v} arises from adiabatic spin transfer torque, and is given by Refs. 36 and 37 as $\mathbf{v} = \frac{gP\mu_B}{-2M_S|e|} \mathbf{J}$, where \mathbf{J} is the current density, $g \approx 2$ is the Landé g factor, M_S is the saturation magnetization, and μ_B denotes the Bohr magneton and e shows the elementary charge. This velocity directly leads to Doppler

shifts in the spin-wave propagation frequency Δf , written as

$$2\pi\Delta f = \mathbf{k} \cdot \mathbf{v} = \frac{gP\mu_B}{-2|e|M_S} \mathbf{J} \cdot \mathbf{k}. \quad (1)$$

As a result, the spin polarization P can be derived from the gradient of a plot of the current-induced frequency shift between opposite spin-wave propagation directions, $2\Delta f$, against current density \mathbf{J} . Previous studies have mostly focused on CIDSD in Permalloy and related films [38], and this technique has not been commonly adopted for evaluations of other materials yet. Here we have investigated CISDS at room temperature for a $\text{Co}_{90}\text{Fe}_{10}$ film, and Ru sandwiched $\text{Co}_{90}\text{Fe}_{10}$ structures as building blocks of synthetic antiferromagnet stacks, alongside a Py film as a control experiment. Three different $\text{Co}_{90}\text{Fe}_{10}$ /Ru structures have been studied in order to study the effects of Oersted fields acting on the $\text{Co}_{90}\text{Fe}_{10}$ caused by vertically asymmetric current distributions.

We adopt a form of propagating spin wave spectroscopy (PSWS) [39,40,41,42] that uses the magnetostatic surface wave (also known as the Damon-Eshbach (DE)) mode [43]. A scanning electron microscopy (SEM) image of a sample appears in the inset of Fig. 1(a), which consists of two electrically isolated short circuit antennas bridged by a ferromagnetic wire, from which they are electrically insulated via a spacer film. The RF-band properties of both antennas are detected by using a 25-GHz vector network analyzer connecting through coplanar waveguides (CPW). The operating principle of PSWS [44] is that the signature of the spin waves is observed as a magnetic resonance behavior in the self-inductance change $\Delta L_{11(22)}$ of the excitation antenna, and also the mutual inductance change $\Delta L_{21(12)}$ between the two antennae. In this paper, we do not need to consider the amplitude of the resonant spectra, and so describe these self and mutual inductance changes using $\Delta S_{11(22)}$ and $\Delta S_{21(12)}$ for simplicity.

All ferromagnetic wires, Ti/Au antennas, and Al_2O_3 insulating spacers were fabricated via conventional lift-off and wet etching processes on thermally oxide silicon wafer. We investigated 5 film structures of wires; single layers of Py ($\text{Ni}_{81}\text{Fe}_{19}$) (20 nm) and of $\text{Co}_{90}\text{Fe}_{10}$ (20) nm, as well as three different Ru / $\text{Co}_{90}\text{Fe}_{10}$ multilayer films: Ru (5 nm) / $\text{Co}_{90}\text{Fe}_{10}$ (10 nm), $\text{Co}_{90}\text{Fe}_{10}$ (10 nm) / Ru (5 nm), and Ru (5 nm) / $\text{Co}_{90}\text{Fe}_{10}$ (10 nm) / Ru (5 nm). The main exchange-coupled wavevectors were set by the antenna dimensions to be 7.85 and $5.22 \mu\text{m}^{-1}$, with $D = 2.6 \mu\text{m}$ in center to center separation distances [45, 46]. The wire width was $4 \mu\text{m}$.

Figure 1(b) shows a typical frequency spectrum of mutual inductance change obtained from Ru / $\text{Co}_{90}\text{Fe}_{10}$ / Ru at applied field $\mu_0 H = +67.5$ mT. The spin wave contribution is isolated by a subtracting reference spectrum taken at $\mu_0 H = \pm 200$ mT. The main peak at 14.0 GHz and a secondary peak at 12.2 GHz correspond to spin-waves coupled two

different wavelengths, and the Fourier transform in Fig. 1(a) gives the corresponding values of wavenumber k . The former coincides with $\lambda \sim 0.8 \mu\text{m}$ ($k_M = 7.85 \mu\text{m}^{-1}$), selected by the center-to-center distance of the CPW, alongside a secondary peak centered at $k_S = 2.80 \mu\text{m}^{-1}$. The spin wave frequency f (shown in Fig. 2) follows the conventional field dependence of the DE mode [47, 48], which is written as

$$f = \frac{\gamma}{2\pi} \mu_0 \left[\sqrt{(H + M_S P_k)(H + M_S(1 - P_k))} \right], \quad (2)$$

where μ_0 is the magnetic permeability of free space, γ is the gyromagnetic ratio, P_k is the dynamic dipole field factor $P_k = 1 - (1 - e^{-|k|t})/|k|t$ and t is the thickness of the ferromagnetic layer. Our experimental results follow this analytical model well, with design parameters of (k_M, k_S) with $\mu_0 M_S = 1.82 \pm 0.01 \text{ T}$ and $g = \gamma \hbar / \mu_B = 2.01 \pm 0.03$, as plotted in Fig. 2. This dispersion relation gives all the material parameters needed to derive the spin polarization P in Eq. 1, and our results for them show good agreement with the typical values reported by previous studies [6, 49].

We have next implemented transmission measurements under a dc current in the wire to study CISDSs. Fig. 3 shows the forward and backward mutual inductance changes measured for a (a) Py and (b) $\text{Co}_{90}\text{Fe}_{10}$ single film wires upon injecting $J = \pm 1.5 \times 10^{11} \text{ A/m}^2$ and $J = \pm 2.0 \times 10^{11} \text{ A/m}^2$ through the wire respectively. Since there is a nonreciprocity of spin-wave coupling in the DE mode [50], S_{12} spectra were taken in positive field ($\mu_0 H = +61.5 \text{ mT}$) whilst S_{21} was measured in negative field ($\mu_0 H = -61.5 \text{ mT}$) to obtain same order major spectra [51]. Therefore, frequency shift in this approach is described as $\Delta f = (f_{12}(+H) - f_{21}(-H))/2$, where $f_{ij}(\pm H)$ denotes the resonant frequency of the $\text{Re}\Delta S_{ij}$ spectra ($i, j = 1, 2$). For the Py wire in Fig. 3(a), the curves show clear shifts horizontally with respect to each other depending on current direction. When positive current is injected (higher panel), the black curve, $\text{Re}\Delta S_{12}$, where spin waves travel in the same direction as the electron flow, is shifted about $17.9 \pm 1.6 \text{ MHz}$ higher than the blue curve $\text{Re}\Delta S_{21}$, where spin waves propagate against the electron flow. When negative current is injected (lower panel), the opposite occurs: the blue curve $\text{Re}\Delta S_{21}$ where spin waves now propagate along the electron flow, is shifted $22.0 \pm 1.0 \text{ MHz}$ higher in frequency than the black one. This is typical behavior of CISDSs, and observed for $\text{Co}_{90}\text{Fe}_{10}$ samples also. The larger magnetization M_S of $\text{Co}_{90}\text{Fe}_{10}$ makes the CISDS in Fig. 3 (b) becomes a little less easy to discern due to the broadening of peak widths and a decrement of value of Δf itself, as described in Eq. 1. The resonant frequencies are determined via Lorentzian curve fitting on the resonant centers, as shown in extensive views of dashed squares next to the whole spectra. This method gives us a precision of 1-2 MHz in the center peak frequency and so we can still

find clear CISDS-type behavior as a $+7.8 \pm 1.1$ MHz shift under the positive current and a -12.2 ± 1.1 MHz shift under the negative current in this figure. Note that the resistance increase due to Joule heating was minimal, with the highest resistance increase for the wire being 2.8%. The corresponding temperature increase lies in range of 5-10 K, small enough that we believe it did not compromise our results significantly. To determine the value of spin polarization using Eq. 1, we plot values of CISDS as Δf normalized by the main wave vector k_M against the electrical current density J for each thin film in Fig. 4(a) and (b). Combining the slope of a line of best fit with the material parameters obtained by the fits to the data in Fig. 2, the spin polarization of our Py film is estimated to be $P = 0.44 \pm 0.03$, and that of our $\text{Co}_{90}\text{Fe}_{10}$ film is $P = 0.33 \pm 0.02$. The result of Py film shows good agreement with other reports of spin Doppler shift results [33, 51] and is also comparable with values obtained by other means [8, 31]. The value for spin polarization of $\text{Co}_{90}\text{Fe}_{10}$ is also quite reasonable.

Fig. 5 shows equivalent plots of normalized values of CISDS $\Delta f/k$ as functions of flowing currents J for our three Ru / $\text{Co}_{90}\text{Fe}_{10}$ multilayer structures. We have taken care to correct account for the effects of Oersted-field induced frequency shifts (OFIFS) for these structures, since current flowing in the Ru layers will exert asymmetric Oersted fields on the $\text{Co}_{90}\text{Fe}_{10}$ layers. First, a nontrivial non-reciprocity becomes important around or above a critical thickness region due to the effect of the exchange interaction [52, 53], which was previously neglected in the standard DE model in Eq. 2. The spin-wave profile decays exponentially away from the surface, and in our case it has an appreciable magnitude throughout the layer, since $k \ll 6\pi/t$, where t is the $\text{Co}_{90}\text{Fe}_{10}$ thickness [52]. Here, the OFIFS effect caused by current in ferromagnetic layers (FLs) can be evaluated through the critical thickness t_c , given in Ref. 52 as $t_c^2 = \alpha_c \pi^2 / (\sqrt{\nu^2 + \nu + 0.5} - \nu - 0.5)$, where $\nu = H/M_S$. In our experiment $\nu = 0.036$ and the exchange constant $\alpha_c = 3.0 \times 10^{-13}$, assuming a Co-like value, which gives $t_c = 39$ nm. In all our measurements the FLs are thinner than this threshold, so that the spin waves are not fully localized at the top or bottom surface of the $\text{Co}_{90}\text{Fe}_{10}$. From this point of view it is reasonable that the effects of OFIFS and the exchange interaction in the FLs should be negligible.

Second, OFIFSs arising from currents flowing in the Ru layers should be still carefully evaluated because our Ru/ $\text{Co}_{90}\text{Fe}_{10}$ bilayer samples are analogous structures to ferromagnet/normal metal bilayer spin interferometers [54, 55] where the OFIFS induced by a current in the Ru layers is generally at least as large as the CISWDS. Accordingly, new values of the Doppler shift are extracted using the following relation: $\Delta f = \{(f_{21}(-I) - f_{21}(+I)) - (f_{12}(-I) - f_{12}(+I))\}/4$, where $f_{ij}(\pm I)$ is determined

from the point where $Re\Delta S_{ij}$ signal ($i, j = 1, 2$) vanishes, prior to the peak maximum.

Without using this four-measurement cancellation method, the apparent frequency shift is as large as $\Delta f \sim 100$ MHz, which drastically exceeds the scale of original CISWDS of around $\Delta f \sim 10$ MHz, and leads to totally unphysical polarizations: $P > 1$ for Ru / Co₉₀Fe₁₀ and $P < -1$ for Co₉₀Fe₁₀ / Ru structures. One notices this sign inversion in P arises from the direction inversion of OFIFS by Ru layers placed above or below the Co₉₀Fe₁₀ layer. The four-measurement evaluation method is designed to cancel out OFIFS by conducting over- or underlayers [56], so long as the first perturbations of OFIFS between f_{12} and f_{21} stay of a comparable size (i.e. $\delta H_{12}(\partial f_{12}/\partial H) \sim \delta H_{21}(\partial f_{21}/\partial H)$), where δH_{ij} is the thickness integrated perturbation of OFIFS. We can further note that a small non-reciprocity between f_{12} and f_{21} in Ref. 53 can be mostly cancelled out by this method, since they are subtracted twice between positive and negative currents. The control measurement of the Co₉₀Fe₁₀ single layer by this method results in the almost perfect agreement of that by the previous evaluation method in Fig. 4, yielding $P = 0.30 \pm 0.03$ (circle data points in Fig. 5). It shows OFIFS cannot be dominant for this single layer sample with this thickness, as already expected from an estimation of critical thickness above.

The results of the bottom Ru sputtered structure Ru (5) / Co₉₀Fe₁₀ (10) are also comparable with that of Co₉₀Fe₁₀ (20) single layer, $P = 0.31 \pm 0.05$, when this new method is used. This good agreement indicates to us that the method of MSSW Doppler shift measures the thickness-integrated spin wave scattering processes, and it is mostly free from interfacial spin density distribution changes, in this case a Ru / Co₉₀Fe₁₀ interface [57].

Meanwhile the structural asymmetry markedly affects the frequency shifts in cases of the top Ru structures Co₉₀Fe₁₀ (10) / Ru (5) and the Ru (5) / Co₉₀Fe₁₀ (10) / Ru (5) trilayer. The extracted frequency shifts no longer follow a linear dependence on J rule in the former, meaning that a reliable value of P cannot be extracted from these data. It also results in large decrement in spin polarization, in the latter, yielding $P = 0.12 \pm 0.01$. The difference between devices with top and bottom Ru comes from stronger current shunting from the Co₉₀Fe₁₀ layer to top Ru layers. The device resistance of a top Ru structure decreases to 76 % of that obtained from a bottom Ru structure, indicating a much lower resistivity for Ru grown on Co₉₀Fe₁₀ than directly onto the substrate. We speculate that this is due to superior crystalline quality in the form of a larger grain size for Ru on top of Co₉₀Fe₁₀. The flow of current in the nonmagnetic layer can be estimated to be 38 % larger on the basis of a simple parallel resistor model. This leads

to a substantial asymmetry in current density in the nominally structurally asymmetric Ru/Co₉₀Fe₁₀/Ru trilayer. Frequency non-reciprocity can be also affected by any difference in surface anisotropies [48, 58]. By substituting $H - (H_{A,top} + H_{A,bottom})$ to the second H in the right hand side of Eq. 2, the anisotropy difference can be estimated as $\Delta H_A = 81.2 \pm 8.7$ mT between the top and bottom Ru structures. There may also be effects arising from interfacial DMI. However, our Ru/CoFe/Ru structure is symmetric, and Ru is a 4d metal and so does not possess a strong spin-orbit coupling. We can therefore expect any DMI to be rather weak and should not lead to a major reduction of polarization due to such an artefact. No meaningful difference of the sort reported in Ref. 48 has been observed in our experiments. Furthermore, our analysis of frequency shifts associated with current inversions should cancel out any DMI-induced changes in the dispersion relations. We have to emphasize that these shunting effects and surface anisotropies cannot quantitatively explain the whole of the reduction of the value of P in the trilayer. A quantitative understanding of this contribution is beyond the scope of this paper because it would require a detailed knowledge of the distribution of spin wave profile and current density over the film thickness.

In summary, we have investigated current-induced spin wave Doppler effects so as to evaluate the spin polarization of Co₉₀Fe₁₀ and Ru / Co₉₀Fe₁₀ multilayer structures. Clear frequency shifts were observed, corresponding to the current injection direction and polarities of spin wave propagation. Values of spin polarizations for Py and Co₉₀Fe₁₀ show good agreement with the general value of each materials. Careful estimation of additional Oersted fields enabled us to deduce polarizations in some cases even in asymmetric structures with non-magnetic Ru under- and overlayers. We believe that this spin-wave spectroscopic technique could be further used to determine spin-polarization values for ordinary diffusive currents in a range of other soft ferromagnetic films.

Acknowledgement

This work was supported by the European Commission through the Marie Curie Fellowship grant No. 627473, SKYHIGH.

References

- [1] S. S. P. Parkin, K. P. Roche, M. G. Samant, P. M. Rice, R. B. Beyers, R. E. Scheuerlein, E. J. O'Sullivan, S. L. Brown, J. Bucchigano, D. W. Abraham, Yu Lu, M. Rooks, P. L. Trouilloud, R. A. Wanner, and W. J. Gallagher, *J. Appl. Phys.* **85**, 5828 (1999).

- [2] S. S. P. Parkin, M. Hayashi, and L. Thomas, *Science* **320**, 5873 (2008).
- [3] J. Z. Sun, *Phys. Rev. B* **62**, 570 (2000).
- [4] P. M. Braganca, J. A. Katine, N. C. Emley, D. Mauri, J. R. Childress, P. M. Rice, E. Delenia, D. C. Ralph, and R. A. Buhrman, *IEEE Trans. Nanotechnol.* **8**, 190 (2009).
- [5] I. W. Wolf, *J. Appl. Phys.* **33**, 1152 (1962).
- [6] S. H. Liao, *IEEE Trans. Magn.* **5**, 2981 (1987).
- [7] A. Yamaguchi, T. Ono, S. Nasu, K. Miyake, K. Mibu, and T. Shinjo, *Phys. Rev. Lett.* **92**, 077205 (2004).
- [8] S. Lepadatu, A. Vanhaverbeke, D. Atkinson, R. Allenspach, and C. H. Marrows, *Phys. Rev. Lett.* **102**, 127203 (2009).
- [9] P. J. Metaxas, J. P. Jamet, A. Mougin, M. Cormier, J. Ferré, V. Baltz, B. Rodmacq, B. Dieny, and R. L. Stamps, *Phys. Rev. Lett.* **99**, 217208 (2007)
- [10] T. Koyama, D. Chiba, K. Ueda, K. Kondou, H. Tanigawa, S. Fukami, T. Suzuki, N. Ohshima, N. Ishiwata, Y. Nakatani, K. Kobayashi and T. Ono, *Nat. Mater.* **10**, 194 (2011).
- [11] L. San Emeterio Alvarez, K.-Y. Wang, S. Lepadatu, S. Landi, S. J. Bending, and C. H. Marrows, *Phys. Rev. Lett.* **104**, 137205 (2010).
- [12] I. Dyaloshinsky, *J. Phys. Chem. Solids.* **4**, 241 (1958).
- [13] T. Moriya, *Phys Rev.* **120**, 91 (1960).
- [14] S. Emori, U. Bauer, S.-M. Ahn, E. Martinez, and G. S. D. Beach, *Nat. Mater.* **12**, 611 (2013).
- [15] K.-S. Ryu, L. Thomas, S.-H. Yang, and S. Parkin, *Nat. Nanotech.* **8**, 527 (2013).
- [16] S. S. P. Parkin, N. More, and K. P. Roche, *Phys. Rev. Lett.* **64**, 2304 (1990).
- [17] H. Yang, K.-S. Ryu, and S. Parkin, *Nat. Nanotech.* **10**, 221 (2015).
- [18] S. Lepadatu, H. Saarikoski, R. Beacham, M. J. Benitez, T. A. Moore, G. Burnell, S. Sugimoto, D. Yesudas, M. C. Wheeler, J. Miguel, S. S. Dhesi, D. McGrouther, S. McVitie, G. Tatara, C. H. Marrows, arXiv: 1604.07992 [cond-mat.mes-hall]
- [19] M. Stokmaier, G. Goll, D. Weissenberger, C. Sürgers, and H. v. Löhneysen, *Phys. Rev. Lett.* **101**, 147005 (2008).
- [20] I. I. Mazin, *Phys. Rev. Lett.* **83**, 1427 (1999).
- [21] D. Mauri, D. Scholl, H. C. Siegmann, and E. Kay, *Phys. Rev. Lett.* **62**, 1900 (1989).
- [22] R. J. Soulen, J. Byers, M. S. Osofsky, B. Nadgorny, T. Ambrose, S. F. Cheng, P. Broussard, C. T. Tanaka, J. Nowak, J. S. Moodera, A. Barry, and J. M. D. Coey, *Science* **282**, 85 (1998).
- [23] S. K. Upadhyay, A. Palanisami, R. N. Louie, and R. A. Buhrman, *Phys. Rev. Lett.*

81, 3247 (1998).

[24] C. H. Shang, J. Nowak, R. Jansen, and J. S. Moodera, *Phys. Rev. B* **58**, R2917 (1998).

[25] B. G. Park, T. Banerjee, B. C. Min, J. G. M. Sanderink, J. C. Lodder, and R. Jansen, *J. Appl. Phys.* **98**, 103701 (2005).

[26] R. Meservey, and P. M. Tedrow, *Phys. Rep.* **238**, 173 (1994).

[27] C. H. Marrows, *Adv. Phys.* **54**, 585 (2005).

[28] J. Bass and W. P. Pratt, Jr., *J. Magn. Magn. Mater.* **200**, 274 (1999).

[29] C. H. Marrows and B. C. Dalton, *Phys. Rev. Lett.* **92**, 097206 (2004).

[30] A. Aziz, S. J. Bending, H. G. Roberts, S. Crampin, P. J. Heard, and C. H. Marrows *Phys. Rev. Lett.* **97**, 206602 (2006).

[31] S. Lepadatu, M. C. Hickey, A. Potenza, H. Marchetto, T. R. Charlton, S. Langridge, S. S. Dhesi, and C. H. Marrows, *Phys. Rev. B* **79**, 094402 (2009).

[32] P. Lederer and D. L. Mills, *Phys. Rev.* **148**, 542 (1966).

[33] V. Vlaminck and M. Bailleul, *Science* **322**, 410 (2008).

[34] Y. B. Bazaliy, B. A. Jones, and S.-C. Zhang, *Phys. Rev. B* **57**, R3213 (1998).

[35] J. Fernández-Rossier, M. Braun, A. S. Núñez, and A. H. MacDonald, *Phys. Rev. B* **69**, 174412 (2004).

[36] S. Zhang and Z. Li, *Phys. Rev. Lett.* **93**, 127204 (2004).

[37] A. Thiaville, Y. Nakatani, J. Miltat, and Y. Suzuki, *Europhys. Lett.* **69**, 990 (2005).

[38] R. Thomas, M. Zhu, C. L. Dennis, and R. D. McMichael, *J. Appl. Phys.* **110**, 033902 (2011).

[39] A. G. Gurevich and G. A. Melkov, *Magnetization Oscillations and Waves* (CRC Press, 1996).

[40] D. D. Stancil, *Theory of Magnetostatic Waves* (Springer, New York, 1993).

[41] M. Bailleul, D. Olligs, C. Fermon, and S. O. Demokritov, *Europhys. Lett.* **56** 741 (2001).

[42] M. Bailleul, D. Olligs, and C. Fermon, *Appl. Phys. Lett.* **83**, 972 (2003).

[43] R. W. Damon and J. R. Eshbach, *J. Phys. Chem. Solids.* **19**, 308 (1961).

[44] V. Vlaminck and M. Bailleul, *Phys. Rev. B* **81**, 014425 (2010).

[45] T. Manago, K. Yamanoi, S. Kasai, and S. Mitani, *J Appl. Phys.* **117** 17D121 (2015).

[46] C. S. Chang, M. Kostylev, E. Ivanov, J. ding, and A. O. Adeyeye, *Appl. Phys. Lett.* **104**, 032408 (2014).

[47] B. A. Kalinikos and A. N. Slavin, *J. Phys. C: Solid State Phys.* **19**, 7013 (1986).

[48] J. M. Lee, C. Jang, B.-C. Min, S.-W. Lee, K.-J. Lee, and J. Chang, *Nano Lett.* **16**, 62

(2016).

[49] J. Rantschler, Y. Ding, S.-C. Byeon, and C. Alexander Jr., *J. Appl. Phys.* **93**, 6671 (2003).

[50] V. E. Demidov, M. P. Kostylev, K. Rott, P. Krzysteczko, G. Reiss, and S. O. Demokritov, *Appl. Phys. Lett.* **95**, 112509 (2009).

[51] M. Zhu, C. L. Dennis, and R. D. McMichael, *Phys. Rev. B* **81**, 140407R (2010).

[52] M. Haidar, M. Bailleul, M. P. Kostylev, and Y. Lao, *Phys. Rev. B* **89**, 094426 (2014).

[53] O. Gladii, M. Haidar, Y. Henry, M. Kostylev, and M. Bailleul, *Phys. Rev. B* **93**, 054430 (2016).

[54] M. P. Kostylev, A. A. Serga, T. Schneider, B. Leven, and B. Hillebrands, *Appl. Phys. Lett.* **87**, 153501 (2005).

[55] T. Schneider, A. A. Serga, B. Leven, and B. Hillebrands, *Appl. Phys. Lett.* **92**, 022505 (2008).

[56] M. Haidar and M. Bailleul, *Phys. Rev. B* **88**, 054417 (2013).

[57] Y. Ji, A. Hoffmann, J. E. Pearson, and S. D. Bader, *Appl. Phys. Lett.* **88**, 052509 (2006).

[58] B. Hillebrands, *Phys. Rev. B* **41**, 530 (1990).

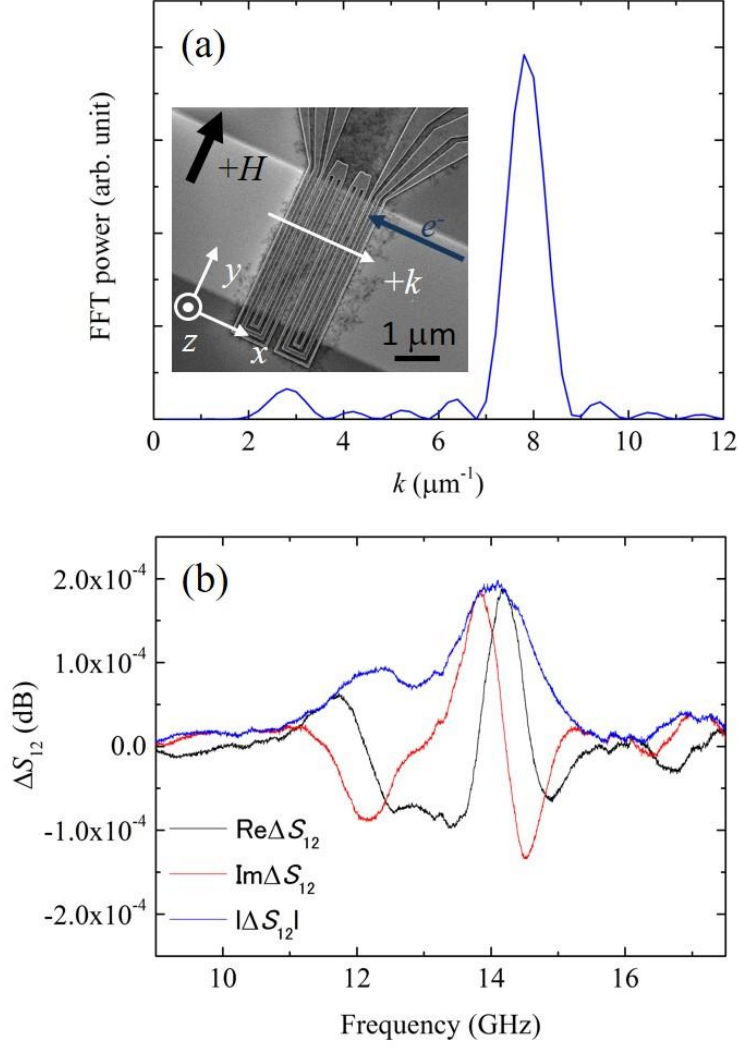


FIG. 1. (Color online). (a) Fourier transform of the microwave current density for antennas by assuming a uniform current density [33, 44]. The antenna geometry defines the main exchange coupled spin wave wavelength to be $0.8 \mu\text{m}$. A SEM image of the corresponding sample is inserted, with a Ru/Co₉₀Fe₁₀/Ru wire ($8 \mu\text{m}$ wide) overlaid by electrically isolated antennas that are connected to the vector network analyzer. (b) Typical resonant spectra of mutual inductance change ΔS_{12} parameter as a function of frequency.

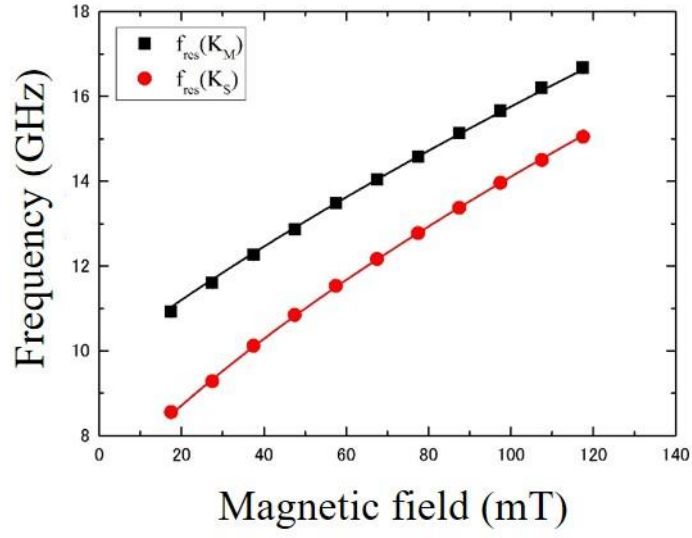


FIG. 2. (Color online). External field dependence of the main ($f_{\text{res}}(k_M)$) and secondary peak frequencies ($f_{\text{res}}(k_S)$). Solid lines are the results of fitting Eq. 2, the DE mode dispersion relation.

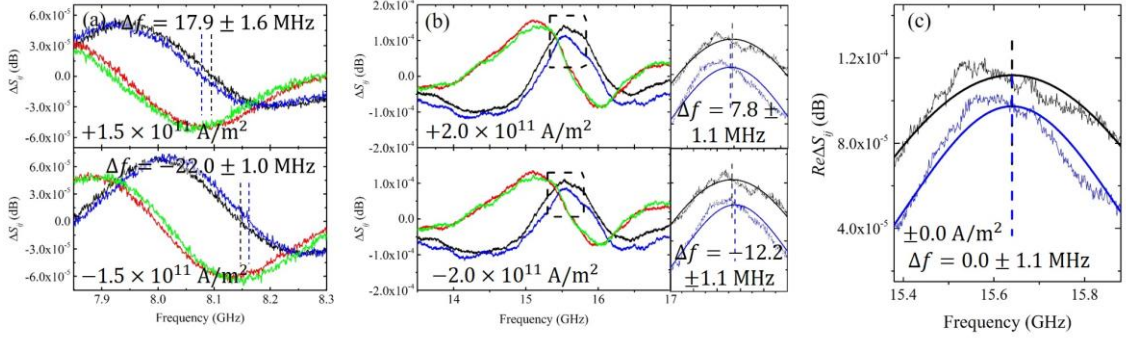


FIG. 3. (Color online). Mutual inductance spectra in the presence of a positive dc current of (a) Py and (b) Co₉₀Fe₁₀ single layer wires. Top sections show results with positive dc current and bottom sections shows that with negative dc current respectively: $J = \pm 1.5 \times 10^{11}$ A/m² for Py and $J = \pm 2.0 \times 10^{11}$ A/m² for Co₉₀Fe₁₀. Black curves show $Re\Delta S_{12}$ and red curves show $Im\Delta S_{12}$, which are measured under the positive field +61.5 mT, and blue curves show $Re\Delta S_{21}$ and green curves shows $Im\Delta S_{21}$, which were measured under the negative field -61.5 mT. The dc electron current passes along $-x$ direction in the upper panel while $+x$ direction in the lower panel. Enlarged views of dashed boxed regions are shown next to each whole spectrum of (b), to illustrate the small CISDSs of Co₉₀Fe₁₀. The results of fitting results Lorentzian curves are superimposed as black and blue solid lines. The vertical dashed lines denote the positions of the fitted peak centers, to specify frequency shift Δf in each spectrum. (c) Enlarged spectra of Co₉₀Fe₁₀ with zero current with Lorentzian fitting (solid lines) and resonant positions (dashed vertical lines), showing no shift.

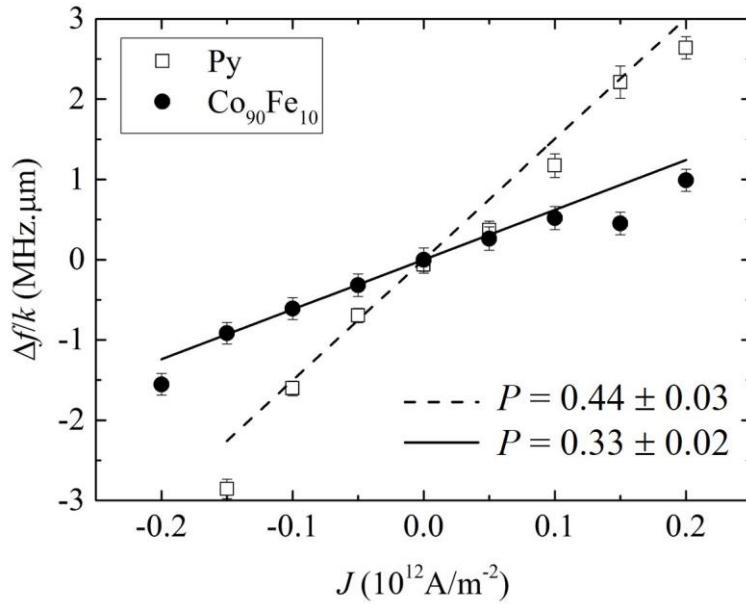


FIG. 4. k -normalized frequency shifts $\Delta f/k$ versus current density J for Py (20), and Co $_{90}$ Fe $_{10}$ (20) wires plotted with open square and circle data point symbols respectively. Superimposed dashed and solid lines show linear fittings with zero intercepts to derive the value of spin polarization P for each films.

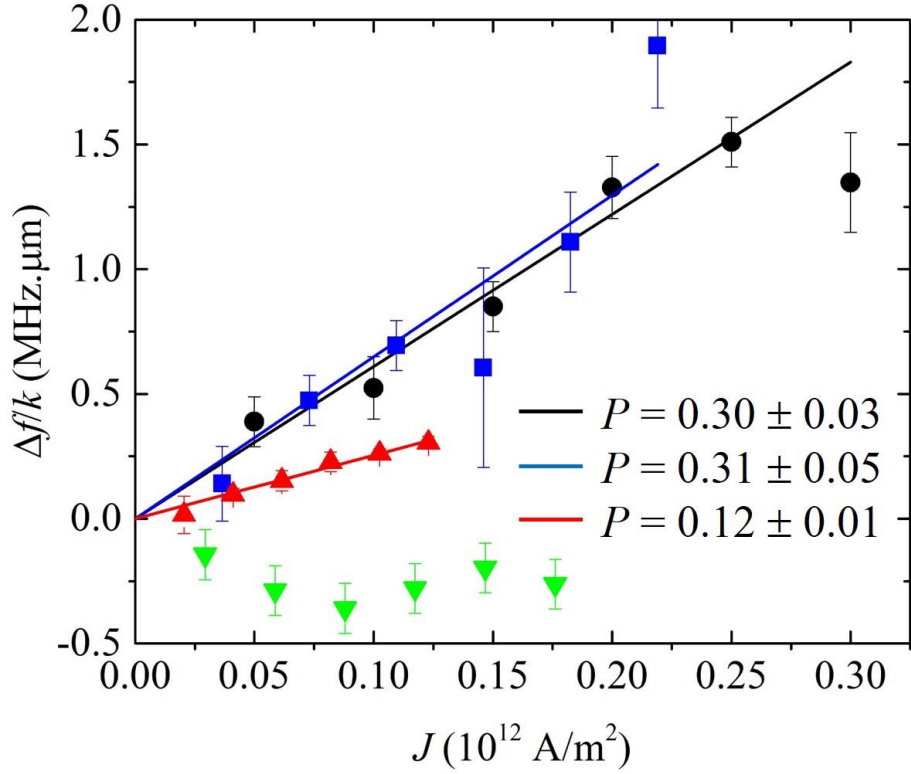


FIG. 5. (Color online). k -normalized frequency shifts Δf versus current density J for $\text{Co}_{90}\text{Fe}_{10}$ (20), Ru (5) / $\text{Co}_{90}\text{Fe}_{10}$ (10), Ru (5) / $\text{Co}_{90}\text{Fe}_{10}$ (10) / Ru (5), $\text{Co}_{90}\text{Fe}_{10}$ (10) / Ru (5) wires plotted with circle, square, triangle, and inverted triangle data point symbols respectively. Superimposed solid lines show lines of best fit with zero intercepts for the first three cases.